Volume 47 | Number 10 | 14 March 2018 | Pages 3195–3598

Dalton Transactions

An international journal of inorganic chemistry

rsc.li/dalton

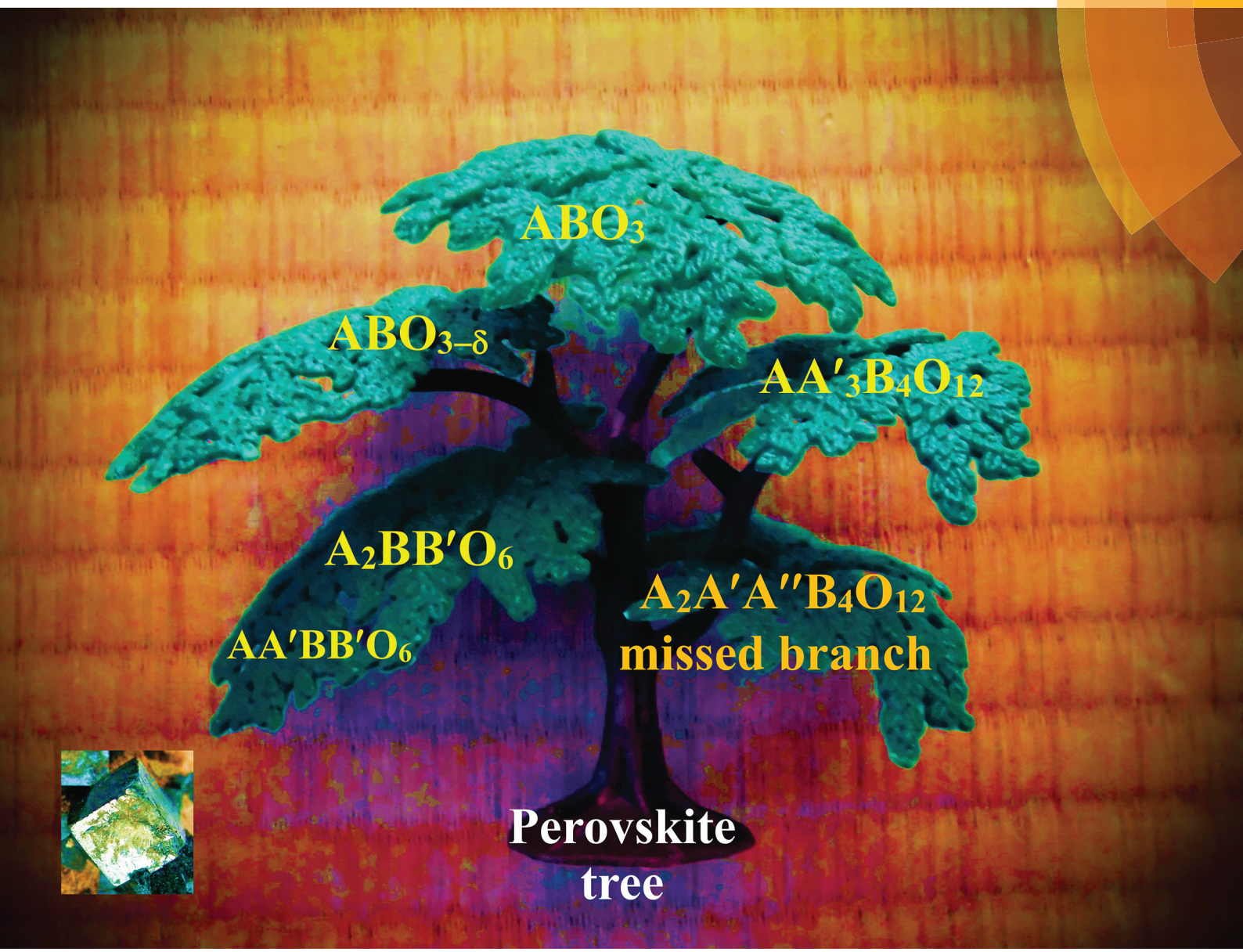

ISSN 1477-9226

ROYAL SOCIETY OF CHEMISTRY

FRONTIER

Alexei A. Belik

Rise of A-site columnar-ordered $A_2A'A''B_4O_{12}$ quadruple perovskites with intrinsic triple order

Dalton Transactions

FRONTIER

View Article Online
View Journal | View Issue

Cite this: *Dalton Trans.*, 2018, **47**, 3209

Rise of A-site columnar-ordered $A_2A'A''B_4O_{12}$ quadruple perovskites with intrinsic triple order

Alexei A. Belik

A-site-ordered $AA'_3B_4O_{12}$ quadruple perovskites (with twelve-fold coordinated A and square-planar coordinated A′ sites) were discovered in 1967. Since then, there have been considerable research efforts to synthesize and characterize new members of such perovskites. These efforts have led to the discoveries of many interesting physical and chemical properties, such as inter-site charge transfer and disproportionation, giant dielectric constant, multiferroic properties, reentrant structural transitions and high catalytic activity. The first member of A-site columnar-ordered $A_2A'A''B_4O_{12}$ quadruple perovskites (with ten-fold coordinated A, square-planar coordinated A′ and tetrahedrally coordinated A″ sites), $CaFeTi_2O_6$, was discovered in 1995, and for 19 years it was the only representative of this family. In the last few years, $A_2A'A''B_4O_{12}$ perovskites have experienced rapid growth. Herein, we present a brief overview of the recent developments in this field and highlight an under-investigated status and great potential of $A_2A'A''B_4O_{12}$, which can be prepared mainly at high pressure and high temperature. The presence of the A″ site gives an additional degree of freedom in designing such perovskites. The $A_2A'A''B_4O_{12}$ perovskites are discussed in comparison with well-known $AA'_3B_4O_{12}$ perovskites.

Received 29th November 2017,
Accepted 14th January 2018

DOI: 10.1039/c7dt04490a

rsc.li/dalton

Research Center for Functional Materials, National Institute for Materials Science (NIMS), Namiki 1-1, Tsukuba, Ibaraki 305-0044, Japan.
E-mail: Alexei.Belik@nims.go.jp

Alexei A. Belik

Alexei Belik graduated from the Department of Materials Science of Moscow State University (MSU), Russia, in 1997 and received his PhD in inorganic chemistry at MSU in 1999. He did his first postdoc (2000–2002) at the National Institute for Materials Science (NIMS), Japan, under the supervision of Prof. Fujio Izumi and his second postdoc (2002–2004) at the Institute for Chemical Research, Kyoto University, under the supervision of Profs. Mikio Takano and Masaki Azuma. In 2004, he joined the NIMS again as an independent scientist under the ICYS program. In 2006, he took a permanent position at the NIMS. He was an MANA independent scientist for 9 years.

Introduction

ABO_3 compounds crystallize in a number of structure types [*e.g.*, perovskites, $LiNbO_3$, corundum, ilmenite, hexagonal $BaMnO_3$-type structures (2*H*, 4*H*, 6*H*, 15*R* and so on), hexagonal $LuMnO_3$-type, pyroxenes, rare earth sesquioxide structures (A, B and C (bixbyite)), $AlFeO_3$, $KSbO_3$, $PbReO_3$, $CaIrO_3$ and others] depending on the relative size of the A and B cations and on the nature of cations.[1] The perovskite-type structure is one of the most important and adaptive structures in inorganic chemistry, and it has the largest number of representatives.[2–4] It is built from a framework of corner-shared BO_6 octahedra that form cavities, which are filled with A cations. The ideal perovskite structure is cubic (space group $Pm\bar{3}m$) with $a_p \approx 3.8$ Å. However, the cubic structure is rarely realized at room temperature because of the mismatch among the sizes of A, B and O. The mismatch, which is usually described by the Goldschmidt tolerance factor,[5] leads to different distortions. Distortions can be considered as tilts of rigid BO_6 octahedra in a first approximation. And tilts, in turn, are described by using the Glazer tilt system and B–O–B bond angles.[6] There are basically 15 tilt systems in ABO_3 perovskites.[4] In simple ABO_3 perovskites, the B–O–B tilt angles are within the range of 140–180°.

A special class of the perovskite family is formed for the $a^+a^+a^+$ tilt system with very large B–O–B tilt angles of about 140–145° (space group of the parent structure is $Im\bar{3}$).[7,8] It is the so-called A-site-ordered quadruple perovskites, $AA'_3B_4O_{12}$,

which have a twelve-fold coordinated A site and a square-planar coordinated A′ site. The A′ site is typically occupied by Jahn–Teller cations [such as, Cu^{2+} and Mn^{3+}] or other cations which allow a square-planar coordination: Cu^{3+},[8] Fe^{2+},[9,10] Co^{2+},[11] Pd^{2+},[12] Pb^{4+} (ref. 13) and Mn^{2+} (ref. 14), and most of the $AA'_3B_4O_{12}$ compounds need high pressure (HP) and high temperature (HT) for their preparation. The $AA'_3B_4O_{12}$ quadruple perovskite subfamily of the perovskite family has also numerous representatives with A = Na^+, Mn^{2+}, Cd^{2+}, Ca^{2+}, Sr^{2+}, Pb^{2+}, R^{3+} (R = rare earths), Ce^{4+}, Bi^{3+} and Th^{4+}, and B = Mn^{3+}, Mn^{4+}, Fe^{3+}, Cr^{3+}, Al^{3+}, Ti^{4+}, V^{4+}, Ge^{4+}, Sn^{4+}, Ru^{4+}, Ir^{4+}, Ta^{5+}, Nb^{5+}, Sb^{5+} and others.[7] This subfamily was discovered in 1967 in $CaCu_3Ti_4O_{12}$ during Cu^{2+} doping of $CaTiO_3$.[15] Since then, there have been considerable research efforts to synthesize and characterize new members of such quadruple perovskites. These efforts have led to the discoveries of many interesting physical and chemical properties, for example, giant dielectric constant,[7] inter-site charge transfer and disproportionation,[8] multiferroic properties, reentrant structural transitions,[16] and high catalytic activity.[17]

Another special class of the perovskite family can be formed with the $a^+a^+c^-$ tilt system and with very large B–O–B tilt angles of about 140–150° (space group of the parent structure is $P4_2/nmc$).[3,4] In such a case, compounds with the $A_2A'A''B_4O_{12}$ stoichiometry are formed. Therefore, they can also be called A-site-ordered quadruple perovskites, where A′ is the site with a square-planar coordination and A″ is the site with a tetrahedral coordination. To distinguish them from $AA'_3B_4O_{12}$, we suggest calling them A-site columnar-ordered[18] quadruple perovskites. The first representative of this subfamily, $CaFeTi_2O_6$, was discovered just in 1995.[9,19,20] $CaFeTi_2O_6$ was the only representative of such quadruple perovskites for 19 years, and this distortion of perovskites was considered to be highly exotic and rare.[3,4] Only in 2014 was another representative reported, $CaMnTi_2O_6$.[21] In the last few years, $A_2A'A''B_4O_{12}$ quadruple perovskites have experienced rapid growth.[18,22–24] The purpose of this frontier article is to highlight their under-investigated status and great potential and to attract attention of the perovskite and high-pressure communities. The $A_2A'A''B_4O_{12}$ quadruple perovskites are compared with the $AA'_3B_4O_{12}$ ones.

Crystal structure descriptions

Simple ABO_3 perovskites can have, and $AA'_3B_4O_{12}$ and $A_2A'A''B_4O_{12}$ quadruple perovskites have very strong tilts of the BO_6 octahedral sublattice with the B–O–B bond angles reaching 140–145°. In simple ABO_3 perovskites, such strong tilts are realized in compounds with quite small A cations, for example, A = Sc and In.[25,26] The ABO_3 perovskites with such strong tilts usually have $GdFeO_3$-related distortions[26] with the (ideal) space group *Pnma* ($\sqrt{2}a_p \times 2a_p \times \sqrt{2}a_p$) and the tilt system of $a^-b^+a^-$, which means that BO_6 octahedra are rotated in one direction (in-phase) along the *b* axis and in opposite directions (out-of-phase) along the *a* and *c* axes (in cubic axes of the original $Pm\bar{3}m$ cell) (Fig. 1a). The $AA'_3B_4O_{12}$ quadruple perovskites have a $2a_p \times 2a_p \times 2a_p$ cell and the $a^+a^+a^+$ tilt system, which means that BO_6 octahedra are rotated in one direction along all three crystallographic directions (Fig. 1b). The $A_2A'A''B_4O_{12}$ quadruple perovskites have a $2a_p \times 2a_p \times 2a_p$ cell and the $a^+a^+c^-$ tilt system, which means that BO_6 octahedra are rotated in one direction along the *a* and *b* axes and in opposite directions along the *c* axis (Fig. 1c). Therefore, on considering the B sublattice, all three perovskites are very similar to each other and differ from each other by a number of the in-phase (very strong) tilts of the BO_6 octahedra.

The different numbers of the in-phase BO_6 tilts (determined, of course, primarily by the stoichiometry) create different numbers and types of cavities for A cations (Fig. 2). There is one type of cavity in the case of ABO_3, and the coordination number is reduced from twelve (in the ideal cubic ABO_3) to eight. The AO_8 polyhedra are connected by edges to form a three-dimensional (3D) network (Fig. 2a).

There are two types of cavities in the case of $AA'_3B_4O_{12}$ with a ratio of 1 : 3. The A site keeps a twelve-fold coordination as in the ideal cubic ABO_3, and the A′ site has four very short A′–O bond lengths, four much longer A′–O bond lengths, and four very long A′–O bond lengths (in total, still twelve). The four very short A′–O bond lengths form a square-planar coordination. The AO_{12} polyhedra are isolated from each other. The $A'O_4$ squares are also isolated from each other (Fig. 2b), and they are oriented in such a way that they are orthogonal to each other, but they are 3D-connected through the longer A′–O bond lengths. The AO_{12} and $A'O_4$ polyhedra are 3D-connected through edges.

There are three types of cavities in the case of $A_2A'A''B_4O_{12}$ with a ratio of 2 : 1 : 1. Therefore, such perovskites have intrinsic triple A-site ordering. The A site has a ten-fold coordination (plus two very long bond lengths), and both A′ and A″ sites have four very short A′–O and A″–O bond lengths with similar values of 1.9–2.1 Å, four much longer bond lengths, and four very long bond lengths (in total, still twelve). The four very short A′–O bond lengths form a square-planar coordination. However, the four very short A″–O bond lengths form a tetrahedral coordination (Fig. 2c). Therefore, the A′ and A″ sites have fundamentally different coordination environments, and they should be distinguished even though they have similar bond lengths. The AO_{10} polyhedra are connected through edges and form chains (columns) along the *c* axis. The $A'O_4$ squares and $A''O_4$ tetrahedra are separated from each other, but they are connected through the longer A′–O bonds to form chains (columns) along the *c* axis. Because of the existence of the $-AO_{10}-AO_{10}-$ columns and the $-A'O_{4+4}-A''O_4-$ columns (or columns consisting of isolated $A'O_4$ and $A''O_4$ units), $A_2A'A''B_4O_{12}$ perovskites can be called A-site columnar-ordered perovskites. Connections of the AO_{10} and $A'O_4$ polyhedra through edges, the AO_{10} and $A''O_4$ polyhedra through corners and the $-AO_{10}-AO_{10}-$ columns through corners create a 3D network. Tetrahedral coordination is usually not realized in oxygen-stoichiometric ABO_3 perovskites; only the removal of oxygen in ordered manners creates tetrahedral sites.[4] The $A_2A'A''B_4O_{12}$

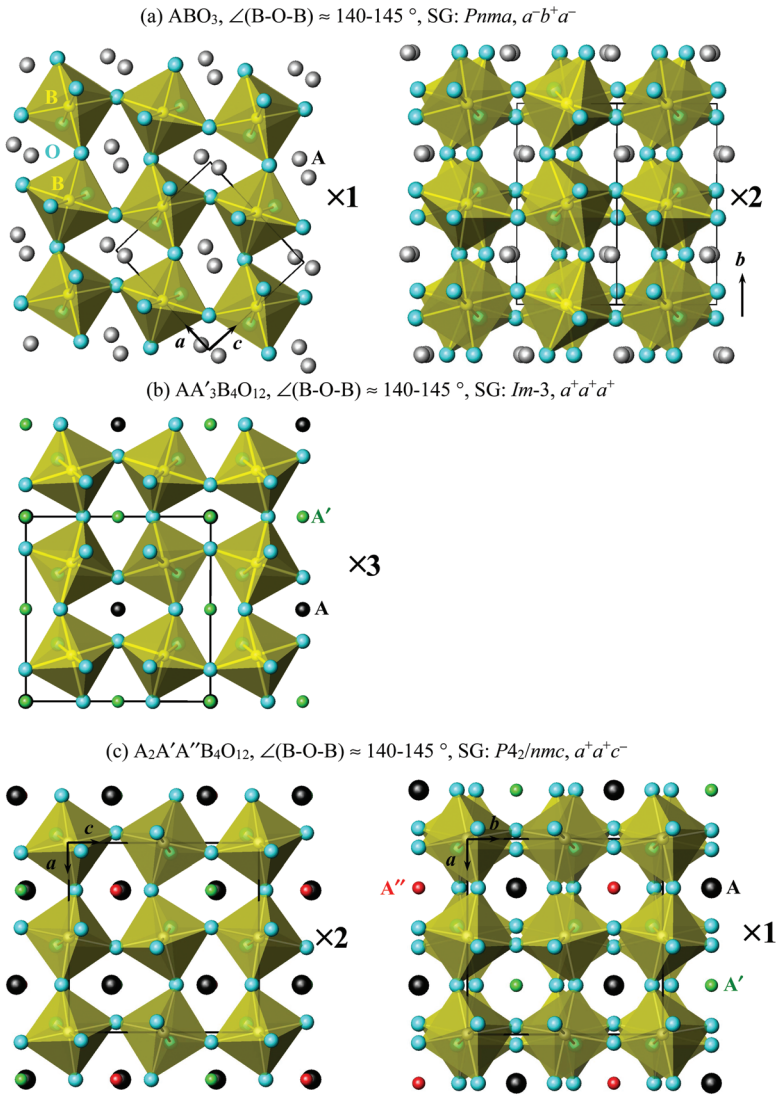

Fig. 1 Connections of BO_6 octahedra along different directions in (a) ABO_3 simple perovskites, (b) $AA'_3B_4O_{12}$ quadruple perovskites and (c) $A_2A'A''B_4O_{12}$ quadruple perovskites, emphasizing different tilt systems. A, A′ and A″ sites are shown by spheres. SG: space group.

perovskites are oxygen-stoichiometric perovskites with tetrahedral sites.

Known examples and expected compositions of $A_2A'A''B_4O_{12}$

The number of reported $A_2A'A''B_4O_{12}$ perovskites is so limited at the moment that they all can be simply listed here (for example, in the chronological order of discovery and in the short formulae): $CaFeTi_2O_6$ (space group $P4_2/nmc$),[9,10,19,20,27] $CaMnTi_2O_6$ (space group $P4_2mc$),[21,28,29] $RMnMnSbO_6$ (R = La, Pr, Nd and Sm) (space group $P4_2/n$),[22] $RMnGaTiO_6$ (R = Sm and Gd) (space group $P4_2/nmc$),[18] $RMnMn_2O_6 \equiv RMn_3O_6$ (R = Gd–Tm and Y) (space group $Pmmn$),[23] $CaMnFeReO_6$,[24] $CaMnMnReO_6$[24] and $Ca_2CuMnFe_2Re_2O_{12}$ (space group $P4_2/n$).[24] We recently prepared $R^{3+}{}_2Mn^{3+}Mn^{2+}[Mn^{3+}{}_3Ti^{4+}]_BO_{12}$ (space group $P4_2/nmc$), $R^{3+}{}_2Mn^{2+}Mn^{2+}[Mn^{3+}{}_2Ti^{4+}{}_2]_BO_{12}$ (space group $P4_2/nmc$), $R^{3+}{}_2Mn^{3+}Ga^{3+}[Mn^{3+}{}_4]_BO_{12}$ (space group $P4_2/nmc$) and $R^{3+}{}_2Cu^{2+}Mn^{2+}[Mn^{3+}{}_2]_{B1}[Mn^{4+}{}_2]_{B2}O_{12}$ (space group $Pmmn$), where $[]_B$ means the presence of one B site and $[]_{B1}[]_{B2}$ means a B-site order.[30] (We note that it was not possible to precisely determine the degree of Cu^{2+} and Mn^{2+} ordering and Mn^{3+} and Ga^{3+} ordering in the last two compounds with X-ray powder diffraction).

Because of the similarities in the B sublattice (Fig. 1), it is expected that the B site of $A_2A'A''B_4O_{12}$ can be occupied by most of the B-type cations for perovskites and their different combinations (a list of examples is given in the second paragraph of Introduction).

The A sites in all three families retain large environments with some variations in the coordination numbers. Therefore, it is expected that the A site of $A_2A'A''B_4O_{12}$ can be occupied by many typical A cations for perovskites (a list of examples is

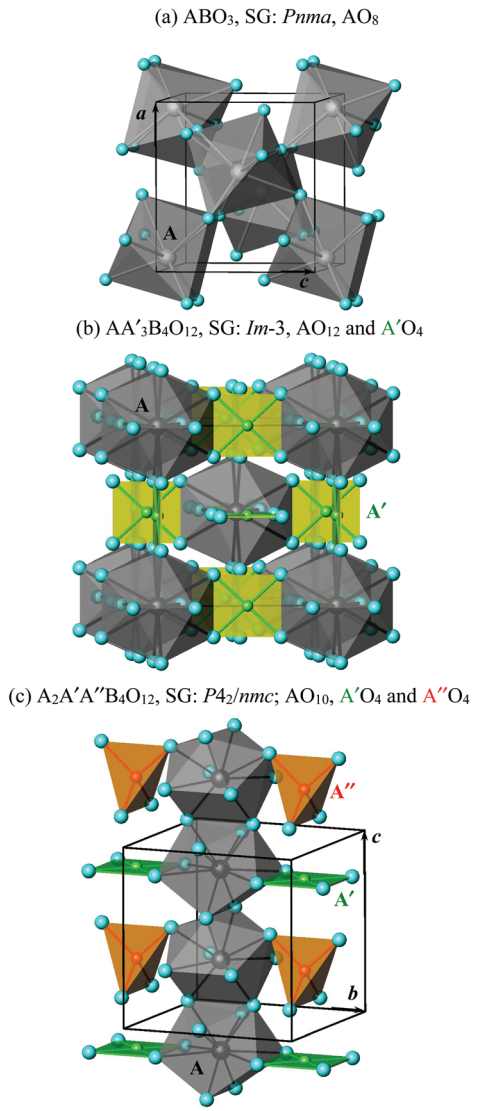

Fig. 2 Fragments of structures with polyhedra for the A, A′ and A″ sites in (a) ABO_3 simple perovskites, (b) $AA'_3B_4O_{12}$ quadruple perovskites and (c) $A_2A'A''B_4O_{12}$ quadruple perovskites. B atoms are omitted for clarity. SG: space group.

given in the second paragraph of Introduction). Despite the twelve-fold coordination of the A site in $AA'_3B_4O_{12}$, we are not aware of any such perovskites with A = Ba^{2+}. This fact shows that strong and almost fixed tilts of the BO_6 octahedra put limits on the possible A–O bond lengths. It is well illustrated by the crystal structures of AMn_7O_{12} with A = Cd, Ca, Sr and Pb,[31,32] where the A–O bond lengths are almost the same in all these compounds (l(A–O) ~ 2.6–2.7 Å) independent of the size of A cations. With high enough pressure, small cations can be forced into the A site resulting in rattling (*e.g.*, in $CuCu_3V_4O_{12}$),[33] while too large cations (*e.g.*, A = Ba) cannot. In $A_2A'A''B_4O_{12}$, the A-site coordination number and A–O bond lengths (l(A–O) ~ 2.3–2.5 Å (×6) and l(A–O) ~ 2.7 Å (×4)) are further reduced in comparison with $AA'_3B_4O_{12}$. This fact can put additional limits on the size of A-type cations that can be forced into the A site. All rare-earth elements (except Ce and Pm) and Ca^{2+} were found so far at the A site of $A_2A'A''B_4O_{12}$. The size of Na^+ is close to those of Ca^{2+} and La^{3+};[34] therefore, we can also expect such compounds with A = Na^+. We also emphasize that depending on compositions at the A′, A″ and B sites, ranges of stability of $A_2A'A''B_4O_{12}$ (A = R = rare-earths) vary from R = La–Sm[22] for $RMnMnSbO_6$ to R = Gd–Tm and Y[23] for $RMnMn_2O_6$ (in all cases, we always mean the synthesis conditions used; stability ranges can change if the synthesis pressure is increased or other conditions are altered). It means that a number of different rare-earth elements should always be checked when preparing such compounds with different B-site contents. A similar tendency was also observed in $AA'_3B_4O_{12}$: for example, $RMn_3(AlTi_3)O_{12}$ is formed for R = La–Sm, but not for R = Gd–Lu;[14] RMn_7O_{12} is formed for R = La–Er and Y, but not for R = Tm–Lu.[23] On the other hand, $RCu_3Mn_4O_{12}$ can be prepared for all R at a relatively low pressure of 2 GPa.[35]

The $A'O_4$ sites of $AA'_3B_4O_{12}$ and $A_2A'A''B_4O_{12}$ are identical. Therefore, it is expected that they can be occupied by the same cations. They are listed and highlighted by bold letters in Table 1, which also gives some other cations with a possible square-planar coordination. We note that there are reports about the presence of Li^+ (*e.g.*, in $(Li_{1.333}Cu_{1.333})Ta_4O_{12}$)[36] and very small amounts of Fe^{3+} and Ti^{4+} at the A′ site of $AA'_3B_4O_{12}$.[37,38] Mn^{3+}, Cu^{2+}, Fe^{2+} and Mn^{2+} were found so far in the A′ site of $A_2A'A''B_4O_{12}$ quadruple perovskites.

The $A''O_4$ tetrahedral site is unique in $A_2A'A''B_4O_{12}$. Table 2 gives a list of some cations that can have a tetrahedral coordination environment and their ionic radii.[34] Cu^{2+}, Fe^{2+} and Mn^{2+} were found so far in the A″ site of $A_2A'A''B_4O_{12}$ and they probably accidentally overlap with cations found at the A′ site (Fig. 3). The charge and size of Co^{2+}, Mg^{2+} and Zn^{2+}, for example, are close to those of Cu^{2+}, Fe^{2+} and Mn^{2+}, but they

Table 1 A list of some cations (in the order of increasing radius) that can have a square-planar oxygen coordination environment[39] and their ionic radii

Cation	Radius (Å)	Cation	Radius (Å)
Cu^{3+}	**≈0.48**	**Fe^{2+}**	**0.64**
Ni^{2+}(LS)	0.49	**Pd^{2+}**	**0.64**
Mn^{3+}	**≈0.51**	**Pb^{4+}**	**0.65**
Cu^{2+}	**0.57**	**Mn^{2+}**	**0.66**
Co^{2+}	**0.58**	Ag^{3+}	0.67
Pt^{2+}	0.60	Au^{3+}	0.68
		Cr^{2+}	Not available

Radii are taken from ref. 34 (for the square-planar (SQ) coordination if available) except for Mn^{3+} and Cu^{3+} ($r_{SQ}(Mn^{3+}/Cu^{3+})$ = l(Mn/Cu–O) – $r(O^{2-})$, where l(Mn–O) = 1.91 Å and l(Cu–O) = 1.88 Å are the average Mn–O and Cu–O bond distances in $AMn^{3+}{}_3B_4O_{12}$ and $ACu^{3+}{}_3B_4O_{12}$ quadruple perovskites (taking the four shortest Mn/Cu–O bonds) and $r(O^{2-})$ = 1.4 Å). Cations marked by bold letters (Cu^{3+}, Mn^{3+}, Cu^{2+}, Co^{2+}, Fe^{2+}, Pd^{2+}, Pb^{4+} and Mn^{2+}) were found in the A′ site of $AA'_3B_4O_{12}$ quadruple perovskites; note that Li^+ (together with Cu^{2+})[36] and very small amounts of Ti^{4+} and Fe^{3+} were also reported.[37,38] Mn^{3+}, Cu^{2+}, Fe^{2+} and Mn^{2+} were found so far in the A′ site of $A_2A'A''B_4O_{12}$ quadruple perovskites. LS: low-spin.

Table 2 A list of some cations (in the order of increasing radius) that can have a tetrahedral oxygen coordination environment[39] and their ionic radii

Cation	Radius (Å)	Cation	Radius (Å)
Ge^{4+}	0.39	**Cu^{2+}**	**0.57**
Al^{3+}	0.39	Co^{2+}(HS)	0.58
Ti^{4+}	0.42	Li^{+}	0.59
Ga^{3+}	0.47	Zn^{2+}	0.60
Fe^{3+}	0.49	**Fe^{2+}(HS)**	**0.63**
Ni^{2+}	0.55	Pb^{4+}	0.65
Sn^{4+}	0.55	**Mn^{2+}(HS)**	**0.66**
Mg^{2+}	0.57	Cd^{2+}	0.78
		Co^{3+}	Not available

Radii are taken from ref. 34. Cations marked by bold letters (Cu^{2+}, Fe^{2+} and Mn^{2+}) were found so far in the A″ site of $A_2A'A''B_4O_{12}$ quadruple perovskites. HS: high-spin.

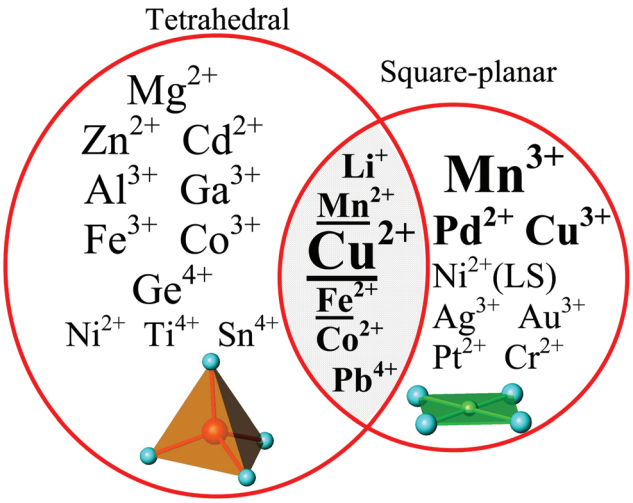

Fig. 3 A schematic figure with some cations that can have a tetrahedral coordination and a square-planar coordination in oxides and their overlap.[39] Bold letters show cations found at the A′ site of $AA'_3B_4O_{12}$. Cu^{2+}, Fe^{2+} and Mn^{2+} (underlined) were found so far in the A″ site of $A_2A'A''B_4O_{12}$ quadruple perovskites.

should preferably occupy the tetrahedral A″ site instead of the square-planar A′ site.[39] On the other hand, however, all cations shown in Table 2 can have an octahedral coordination, and some of them (*e.g.*, Ni^{2+}, Sn^{4+} and Ti^{4+}) show a very strong preference for such an environment.[39] Therefore, strong competitions with the octahedral B sites or the formation of other phases where such cations have an octahedral coordination are possible. One strategy to force them into the A″ site is to use cations at the B sites with an even stronger preference for octahedral environments (similar to $NiCr_2O_4$ and $CuCr_2O_4$ spinels). We can expect that with high enough pressure during the synthesis some elements from Table 2 (in addition to Cu^{2+}, Fe^{2+} and Mn^{2+}) can be stabilized at the A″ site. For example, 5 GPa was enough to stabilize Fe^{2+} in the square-planar A′ site of $CaFe_3Ti_4O_{12}$, while more than 12 GPa was required to prepare $CaFeTi_2O_6$ with Fe^{2+} in both the square-planar A′ and tetrahedral A″ sites.[9]

An attempt to prove the above concept (about the location of different elements at the A′ and A″ sites) was made as shown in ref. 24 by the synthesis of $Ca_2CuMnFe_2Re_2O_{12}$ aiming at Cu^{2+} at the A′ site and Mn^{2+} at the A″ site. We synthesized $R_2CuMnMn_4O_{12}$. We also tried to insert Ga^{3+} and prepared $R_2MnGaMn_4O_{12}$ (space group $P4_2/nmc$).[30] We emphasize that because Mn^{3+} can disproportionate during the synthesis as found in $RMnMn_2O_6$ = $[R^{3+}{}_2]_A[Mn^{3+}]_{A'}[Mn^{2+}]_{A''}[Mn^{3+}{}_2]_{B1}[Mn^{3+}Mn^{4+}]_{B2}O_{12}$,[23] any cation/charge distributions are possible between $[R^{3+}{}_2]_A[Mn^{3+}]_{A'}[Ga^{3+}]_{A''}[Mn^{3+}{}_4]_BO_{12}$ with Ga^{3+} at the A″ site and $[R^{3+}{}_2]_A[Mn^{3+}]_{A'}[Mn^{2+}]_{A''}[Mn^{3+}{}_2Mn^{4+}Ga^{3+}]_BO_{12}$ with Ga^{3+} at the B site (assuming[39] that the A″ site cannot be occupied by Mn^{3+} and Mn^{4+}). Our structural analysis with X-ray powder diffraction data gave evidence that the cation distribution is more close to the former case (A″–O bond lengths of 1.89 Å were more consistent with Ga–O bond lengths). However, a precise model can only be determined with neutron diffraction, and this method is an essential tool to study cation distributions in $A_2A'A''B_4O_{12}$.

The presence of the A″ site gives an additional degree of freedom in $A_2A'A''B_4O_{12}$, and the number of elements that can have a tetrahedral environment is larger than that with a square-planar environment (Fig. 3). Therefore, it is expected that $A_2A'A''B_4O_{12}$ perovskites should be numerous and versatile.

Known distortions

The parent structure of $AA'_3B_4O_{12}$ has the space group $Im\bar{3}$ (no. 204). All distortions from the direct group–subgroup relations are experimentally realized (except for the same $Im\bar{3}$ symmetry with $6a_p \times 6a_p \times 6a_p$) (Fig. 4). These distortions are exemplified in $CaCu_3Ti_4O_{12}$ (the parent structure),[15,40] $CaCu_3Ga_2Sb_2O_{12}$,[41] $Ce_{0.5}Cu_3Ti_4O_{12}$,[42] $(Li_{1.333}Cu_{1.333})Nb_4O_{12}$,[36] $CaCu_3Fe_4O_{12}$,[8,38] $A^{2+}Mn_7O_{12}$ (A = Cd, Ca, Sr and Pb)[31,32] and $BiCu_{0.2}Mn_{6.8}O_{12}$.[16] Most of these distortions are temperature-driven, that is, they are observed on cooling for a particular composition, and there exists a high-temperature parent modification. However, there are a few composition-driven distortions, that is, they are determined by a particular composition and take place during the synthesis.[41,42] The $I23$ distortion in $(Li_{1.333}Cu_{1.333})Nb_4O_{12}$ could be temperature-driven (caused by Nb displacements), but no evidence (no phase transitions to the parent structure) was reported;[36] this is why we call it composition-driven. There are a number of temperature-driven distortions that cannot be described by the direct group–subgroup paths, for example, in $LaMn_7O_{12}$ ($Im\bar{3} \Rightarrow (Immm) \Rightarrow I2/m$),[43] $NaMn_7O_{12}$ ($Im\bar{3} \Rightarrow (Immm) \Rightarrow (I2/m) \Rightarrow C2/m$)[44,45] and $BiMn_7O_{12}$ ($Im\bar{3} \Rightarrow (Immm) \Rightarrow I2/m \Rightarrow Im \Rightarrow I1$),[46] and there is one such composition-driven distortion in $Cu_{2+x}Ta_4O_{12}$ ($Im\bar{3} \Rightarrow (Pm\bar{3}) \Rightarrow Pmmm$),[47] where space groups in parentheses give group–subgroup links. Despite a large number of $AA'_3B_4O_{12}$-type compounds, proper polar distortions are realized only in one case of $BiMn_7O_{12}$ due

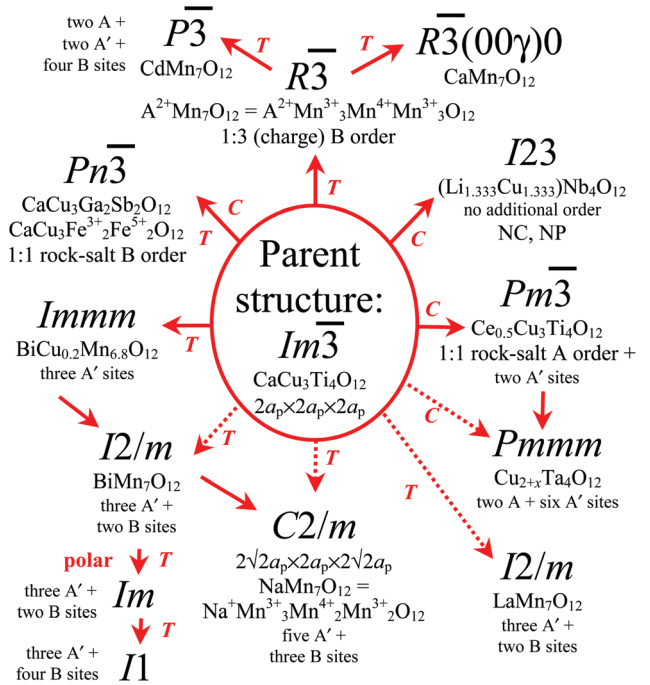

Fig. 4 A schematic diagram of all direct group–subgroup distortions and other known distortions of the parent structure of $AA'_3B_4O_{12}$ quadruple perovskites (space group $Im\bar{3}$). Direct group–subgroup distortions are shown by solid arrows; other distortions are shown by dashed arrows. Examples of known distortions are given. Types of A- and B-site orders or number of distinct sites are highlighted. All distortions keep the $2a_p \times 2a_p \times 2a_p$ cell except $R\bar{3}$, $P\bar{3}$, $R\bar{3}(00\gamma)0$ and $C2/m$. *T*: a temperature-driven distortion, *C*: a composition-driven distortion, NC: non-centrosymmetric, NP: non-polar.

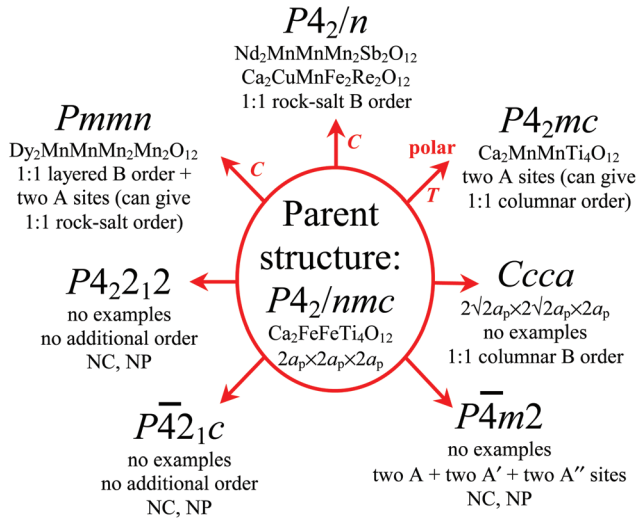

Fig. 5 A schematic diagram of all direct group–subgroup distortions of the parent structure of $A_2A'A''B_4O_{12}$ quadruple perovskites (space group $P4_2/nmc$). Examples of known distortions are given. Types of A- and B-site orders or number of distinct sites are highlighted. All distortions keep the $2a_p \times 2a_p \times 2a_p$ cell except *Ccca*. *T*: a temperature-driven distortion, *C*: a composition-driven distortion, NC: non-centrosymmetric, NP: non-polar.

to the effects of the lone electron pair of Bi^{3+}.[46] But the ferroelectricity of $BiMn_7O_{12}$ has not been demonstrated yet.

The parent structure of $A_2A'A''B_4O_{12}$ has the space group $P4_2/nmc$ (no. 137). There are seven distortions from the direct group–subgroup relations (except for the same $P4_2/nmc$ symmetry with $2a_p \times 2a_p \times 6a_p$ and $6a_p \times 6a_p \times 2a_p$) (Fig. 5). Three of them have already been found experimentally. Surprisingly, a temperature-driven proper polar distortion takes place in $CaMnTi_2O_6$ without any effects of lone electron pairs.[21] This is a quite promising fact in comparison with the $AA'_3B_4O_{12}$ family. Rock-salt B-site (space group $P4_2/n$)[22,24] and layered B-site (space group $Pmmn$)[23] orders have already been realized in $A_2A'A''B_4O_{12}$. The reported $P4_2/n$ distortion is composition-driven. The $Pmmn$ distortion in $RMnMn_2O_6$ could be temperature-driven, but no evidence (no phase transitions to the parent structure) was found so far; this is why we call it composition-driven. It is interesting that the $Pmmn$ model has potential for an additional 1 : 1 rock-salt A-site order (that is, it has two independent A sites: A1 and A2), which might be realized, for example, in a hypothetical compound $[Ca^{2+}]_{A1}[Dy^{3+}]_{A2}[Mn^{3+}]_{A'}[Mn^{2+}]_{A''}[Mn^{3+}{}_2]_{B1}[Mn^{4+}{}_2]_{B2}O_{12}$ (it is just given to illustrate compositional design principles). The polar $P4_2mc$ distortion has potential for an additional 1 : 1 columnar A-site order: $[Na^{+}]_{A1}[Nd^{3+}]_{A2}[Mn^{2+}]_{A'}[Mn^{2+}]_{A''}[Ti^{4+}{}_4]_BO_{12}$ (a hypothetical compound to illustrate compositional design principles). A1–O and A2–O distances in the $Pmmn$ (*e.g.*, $RMnMn_2O_6$) and $P4_2mc$ (*e.g.*, $CaMnTi_2O_6$) models are different; therefore, there might be driving forces for the ordering of cations with different oxidation states and sizes. The rock-salt A-site ordering is rare in ABO_3;[3,4] however, the ordering would not be direct in the $Pmmn$ model because the A sublattice is 'diluted' by A′ and A″.

Physical and chemical properties of $A_2A'A''B_4O_{12}$

As already mentioned, $CaMnTi_2O_6$ crystallizes in a polar space group. This compound shows a structural phase transition from $P4_2mc$ to the parent $P4_2/nmc$ structure at 630 K. The phase transition is accompanied by sharp dielectric constant anomalies and the loss of second-harmonic generation signals. Moreover, a room-temperature ferroelectric P–E hysteresis loop was demonstrated.[21] These results proved that $CaMnTi_2O_6$ is ferroelectric at a ferroelectric Curie temperature of 630 K. The shifts of Mn^{2+} cations at the A′ site from the square-planar plane and Ti^{4+} cations from the center of the TiO_6 octahedra are responsible for the polar distortion.[21,29] Polarization was calculated to be about 0.3 C m^{-2}, and a highly tunable semiconducting energy band gap was predicted in $CaMnTi_2O_6$.[29] The $P4_2mc$-to-$P4_2/nmc$ ferroelectric transition was also found at room temperature at about 7 GPa.[28]

Without the assistance from the B sublattice, the interaction among magnetic cations at the A′ and A″ sites is usually very weak (at least, among Mn^{2+}): $CaMnTi_2O_6$ has the Néel

temperature ($T_{A,N}$) of about 10 K,[21] while $SmMnGaTiO_6$ was reported to order at $T_{A,N}$ = 3 K, and no ordering was found in $GdMnGaTiO_6$.[18] In the case of $SmMnGaTiO_6$ and $GdMnGaTiO_6$, even small disordering of Ga^{3+} and Mn^{2+} between the A″ and B sites could suppress a long-range magnetic ordering. On the other hand, magnetic interactions through Ti^{4+} could be enhanced in $CaMnTi_2O_6$ resulting in higher T_N similar to a higher magnetic transition temperature in $CaCu_3Ti_4O_{12}$ in comparison with $CaCu_3Ge_4O_{12}$ and $CaCu_3Sn_4O_{12}$.[3] No cooperative long-range magnetic order of the parent compound, $CaFeTi_2O_6$, was found down to 4.2 K.[27]

The presence of magnetic cations at the B sites significantly enriched magnetic behaviours. First, the ordering temperature of Mn^{2+} at the A′ and A″ sites can reach $T_{A,N}$ = 70 K in $CaMnFeReO_6$ [24] and $T_{A,C}$ = 100 K in $CaMnMnReO_6$.[24] Second, the magnetic ordering of Mn^{2+} at the A′ and A″ sites can be either antiferromagnetic ($T_{A,N}$ in $CaMnFeReO_6$)[24] or ferromagnetic ($T_{A,C}$ in $CaMnMnReO_6$ [24] and T_C = 76 K in $NdMnMnSbO_6$).[22] Magnetic cations at the B sublattice can order first as in $CaMnMnReO_6$ at $T_{B,C}$ = 120 K (a ferrimagnetic structure),[24] can order first with much higher temperatures as in $CaMnFeReO_6$ at $T_{B,C}$ = 500 K and in $Ca_2CuMnFe_2Re_2O_{12}$ at $T_{B,C}$ = 560 K (a ferrimagnetic structure of Fe^{3+} and Re^{5+})[24] or can order at the same temperature with the A′ and A″ sites as in $NdMnMnSbO_6$.[22] There is a spin reorientation transition in $NdMnMnSbO_6$ at 42 K driven by order of the Nd moments.[22] $RMnMn_2O_6$ compounds also show complex magnetic behaviours at several transition temperatures (two or three magnetic transitions depending of R and stoichiometry);[23] but magnetic structures have not been investigated yet. The maximum magnetic transition temperature is about 80 K in $RMnMn_2O_6$,[23] but it jumps to about 180 K in $R_2CuMnMn_4O_{12}$ after Cu^{2+} doping.[30] This jump could be caused by the increase of the Mn^{4+} concentration at one of the B sites from $[Mn^{3+}{}_2]_{B1}[Mn^{3+}Mn^{4+}]_{B2}$ to $[Mn^{3+}{}_2]_{B1}[Mn^{4+}{}_2]_{B2}$. Most of the $R_2CuMnMn_4O_{12}$ compounds exhibit three magnetic transitions (*e.g.*, at 15, 145 and 180 K for R = Tm).[30] Significant magnetoresistance was found in $CaMnFeReO_6$ and magnetoresistance switching was observed in $Ca_2CuMnFe_2Re_2O_{12}$.[24] Therefore, $A_2A'A''B_4O_{12}$ perovskites show complex magnetic properties.

It was found that $RMnMn_2O_6$ ($\equiv RMn_3O_6$) compounds are prone to non-stoichiometry, $R_{1-\delta}Mn_3O_{6-1.5\delta}$, with δ = −(0.059–0.071) for R = Gd, δ = 0 for R = Dy, δ = 0.05–0.1 for R = Ho and Y, and δ = 0.12 for R = Er and Tm, and their magnetic properties are highly sensitive to the δ values.[23] The real rare-earth cation deficiency was formed in the case of $Er_{0.88}Mn_3O_{5.82}$ and $Tm_{0.88}Mn_3O_{5.82}$; and the cation distribution can be written as $[Tm^{3+}{}_{1.76}]_A[Mn^{3+}]_{A'}[Mn^{2+}]_{A''}[Mn^{3+}{}_2]_{B1}[Mn^{3+}Mn^{4+}]_{B2}O_{12-\delta}$.[30] However, the manganese deficiency in $GdMn_{3-y}O_{6-1.5y}$ is realized through the doping of a small amount of Gd into the tetrahedral A″ site: $[Gd^{3+}{}_2]_A[Mn^{3+}]_{A'}[Mn^{2+}{}_{0.86}Gd^{3+}{}_{0.14}]_{A''}[Mn^{3+}{}_2]_{B1}[Mn^{3.43+}{}_2]_{B2}O_{12}$.[30] The location of rare-earth elements at tetrahedral sites is very unusual.[39] $RMnMn_2O_6$ compounds were prepared from R_2O_3 and $Mn^{3+}{}_2O_3$.[23] However, during the synthesis at HP and HT, charge disproportionation takes place because Mn can enter the A″ site only in the oxidation state of +2.

Neutron diffraction showed that Fe^{3+} cations occupy the A′ site (8%) and the A″ site (16%) in $CaMnFeReO_6$.[24] This fact shows that Fe^{3+} can in principle be at the tetrahedral A″ site (Fig. 3). The location of a very small amount of Fe^{3+} cations at the square-planar A′ site was also observed in $AA'_3B_4O_{12}$ by Mössbauer spectroscopy, but the concentration never reaches a few percent.[38] A very small antisite disorder at the B sites was found in $CaMnFeReO_6$ (3% Fe/Re) and $CaMnMnReO_6$ (4% Mn/Re); $CaMnMnReO_6$ also had about 5% of Mn at the Ca site,[24] and small amounts of Mn were found at the Nd and Sb sites of $NdMnMnSbO_6$.[22]

Different atoms (*e.g.*, Cu^{2+} and Mn^{2+}) that can occupy both tetrahedral and square-planar sites (Fig. 3) order poorly between the A′ and A″ sites as found by neutron diffraction in the case of $Ca_2CuMnFe_2Re_2O_{12}$ (60% Cu and 40% Mn at A′ and 23–36% Cu and 64–77% Mn at A″);[24] and the degree of ordering can depend on synthesis conditions.[24] On the other hand, different charge orderings take place (at the A′ and A″ sites and/or at the B site) for the same atom; examples with Mn known so far are: $RMnMn_2O_6$, $R_2MnMn[Mn_3Ti]_BO_{12}$ and $R_2CuMnMn_4O_{12}$. Mn^{2+} and Mn^{3+} at the A′ site can be distinguished by Mn–O bond lengths: $l(Mn^{2+}\text{–}O) \sim 2.1$ Å and $l(Mn^{3+}\text{–}O) \sim 1.91$ Å. Other good candidates for such same-atom charge-ordered scenarios are Cu, Co and Fe (Fig. 3). Another interesting observation is that when the B site is solely occupied by Mn with the average oxidation state higher than +3, there seems to be a tendency for a layered B-site ordering with the appearance of one layer consisting of highly distorted (by the Jahn–Teller effect) $Mn^{3+}O_6$ octahedra.

Very few compositions of $AA'_3B_4O_{12}$ can be prepared at ambient pressure (for example, $(Li_{1.333}Cu_{1.333})Nb_4O_{12}$,[36] $Cu_{2+x}Ta_4O_{12}$,[47] $CaMn_7O_{12}$ and $CaCu_3Ti_4O_{12}$).[3] The majority of $AA'_3B_4O_{12}$ requires HP and HT synthesis conditions. All known $A_2A'A''B_4O_{12}$ require HP and HT conditions. They were prepared at 12 GPa–1670 K for $CaFeTi_2O_6$,[20] 7 GPa–1470 K for $CaMnTi_2O_6$,[21] 10 GPa–1470 K for $RMnMnSbO_6$,[22] 6 GPa–1370 K for $RMnGaTiO_6$,[18] 6 GPa–1670 K for $RMnMn_2O_6$,[23] and 10 GPa–1670 K for $CaMnFeReO_6$ (and others).[24]

The symmetry of $A_2A'A''B_4O_{12}$ under synthesis conditions is crucial for the realization of ordering of different cations between the A′ and A″ sites. In general, three situations are possible for compounds with the $A_2A'A''B_4O_{12}$ stoichiometry. First, the structure can have one crystallographic A site (*e.g.*, with the maximum symmetry of $Pm\bar{3}m$ and $a_p \times a_p \times a_p$). In this case, we will probably have $GdFeO_3$-type structures (simple ABO_3 perovskites) with random distribution of all A cations at one site after quenching and pressure release.[22] Second, the structure can have two crystallographic A sites with the 1 : 1 ratio (*e.g.*, with *P*4/*mmm* symmetry and $\sqrt{2}a_p \times \sqrt{2}a_p \times a_p$ considered in ref. 29). In this case, it is difficult to expect noticeable ordering of different cations between the A′ and A″ sites. Third, the structure can have three A sites with the 2 : 1 : 1 ratio (*e.g.*, with *I*4/*mmm* symmetry and $2a_p \times 2a_p \times 2a_p$). In this case,

the ordering of different cations between the A′ and A″ sites can be realized. If the second case takes place (for some compositions), a modification of synthesis conditions could help to increase the ordering. In most cases, samples are quenched after the synthesis, but slow cooling could drive (partial) ordering. We are not aware of any *in situ* HP and HT studies of either $AA'_3B_4O_{12}$ or $A_2A'A''B_4O_{12}$.

Some arguments in favor of the terminology

The $AA'_3B_4O_{12}$ and $A_2A'A''B_4O_{12}$ quadruple perovskites have many common structural features (Fig. 1 and 2). The parent structures of both families have the doubled lattice parameter along all three crystallographic directions, $2a_p \times 2a_p \times 2a_p$, in comparison with a simple ABO_3 perovskite with $a_p \approx 3.8$ Å resulting in eight ABO_3 formula units in their unit cell. The simplest composition with integer numbers can be written as $AA'_3B_4O_{12}$ ($Z = 2$), corresponding to four ABO_3 units. This is why such perovskites are called quadruple. This formula reflects the presence of the A and A′ cations with quite different coordination environments with the 1 : 3 ratio. Because 1 and 3 are odd numbers (and A and A′ are quite different cations), this formula is retained in the majority of cases. However, there are very few exceptions when A′ = A (for example, $CuCu_3V_4O_{12}$ and $MnMn_3Mn_4O_{12}$).[33,48] For such cases, the formula can be reduced to simple ABO_3 ($Z = 8$). However, this formal formula reduction does not eliminate the structural features of such perovskites – they still belong to the A-site-ordered quadruple perovskite family. Note that perovskites and perovskite-related compounds with the 1 : 3 B-site ordering can also be referred to as (B-site-ordered) quadruple perovskites.[49,50] By analogy, the simplest composition with integer numbers can be written as $A_2A'A''B_4O_{12}$ ($Z = 2$), which reflects quite different coordination environments for the A, A′ and A″ sites with the 2 : 1 : 1 ratio. The $A_2A'A''B_4O_{12}$ formula corresponds to quadruple perovskites. It turns out that A″ = A′ in many cases for perovskites reported so far, and the formula can be reduced to the double perovskite one, $AA'B_2O_6$. However, this formal formula reduction does not reflect the structural features of such perovskites, which still belong to the A-site columnar-ordered quadruple perovskite family, $A_2A'A''B_4O_{12}$. $Ca_2CuMnFe_2Re_2O_{12}$,[24] $R_2CuMnMn_2Mn_2O_{12}$ (or $R_2CuMn_5O_{12}$)[30] and $R_2MnGaMn_4O_{12}$ (or $R_2GaMn_5O_{12}$)[30] already require the quadruple formula to write them in integer numbers.

Conclusion

A-site columnar-ordered $A_2A'A''B_4O_{12}$ quadruple perovskites are in the incipient stage of research. They can be considered as an extended and more complex version of the A-site-ordered $AA'_3B_4O_{12}$ quadruple perovskites (with twelve-fold coordinated A and square-planar coordinated A′ sites) because $A_2A'A''B_4O_{12}$ has ten-fold coordinated A and square-planar coordinated A′ sites plus an additional tetrahedrally coordinated A″ site. This A″ site gives an additional degree of freedom in $A_2A'A''B_4O_{12}$ because the number of elements that can have a tetrahedral environment is larger than that with a square-planar environment. The $A_2A'A''B_4O_{12}$ perovskites are the only oxygen-stoichiometric perovskites with tetrahedral sites. This article highlights great potential of $A_2A'A''B_4O_{12}$ and gives some design principles.

Note added in proof

After this paper was accepted, the synthesis of ferroelectric $Ca_{2-x}Mn_xTi_2O_6$ ($x = 0.6$) by a spark plasma sintering method was reported.[51]

Conflicts of interest

There are no conflicts to declare.

Acknowledgements

This work was partially supported by JSPS KAKENHI Grant Numbers JP15K14133 and JP16H04501 and JSPS Bilateral Open Partnership Joint Research Projects. We thank Mr L. Zhang (NIMS), Dr Y. Matsushita (NIMS) and Dr K. Yamaura (NIMS) for their help with unpublished experimental data mentioned in this article and Profs. E. V. Antipov (Moscow State University) and I. A. Presniakov (Moscow State University) for discussion.

References

1 D. M. Giaquinta and H.-C. zur Loye, *Chem. Mater.*, 1994, **6**, 365–372.
2 R. H. Mitchell, *Perovskites: Modern and Ancient*, Almaz Press, Thunder Bay, Ontario, Canada, 2002.
3 G. King and P. M. Woodward, *J. Mater. Chem.*, 2010, **20**, 5785–5796.
4 A. M. Abakumov, A. A. Tsirlin and E. V. Antipov, Transition-Metal Perovskites, in *Comprehensive Inorganic Chemistry II (Second Edition): From Elements to Applications*, ed. J. Reedijk and K. R. Poeppelmeier, Elsevier, Amsterdam, 2013, vol. 2, pp. 1–40.
5 V. M. Goldschmidt, *Naturwissenschaften*, 1926, **14**, 477–485.
6 A. M. Glazer, *Acta Crystallogr., Sect. A: Cryst. Phys., Diffr., Theor. Gen. Crystallogr.*, 1975, **31**, 756–762.
7 A. N. Vasil'ev and O. S. Volkova, *Low Temp. Phys.*, 2007, **33**, 895–914.
8 I. Yamada, *J. Ceram. Soc. Jpn.*, 2014, **122**, 846–851.
9 K. Leinenweber, J. Linton, A. Navrotsky, Y. Fei and J. B. Parise, *Phys. Chem. Miner.*, 1995, **22**, 251–258.

10 J. Linton, A. Navrotsky and Y. Fei, *Phys. Chem. Miner.*, 1998, **25**, 591–596.
11 S. V. Ovsyannikov, Y. G. Zainulin, N. I. Kadyrova, A. P. Tyutyunnik, A. S. Semenova, D. Kasinathan, A. A. Tsirlin, N. Miyajima and A. E. Karkin, *Inorg. Chem.*, 2013, **52**, 11703–11710.
12 K. Shiro, I. Yamada, N. Ikeda, K. Ohgushi, M. Mizumaki, R. Takahashi, N. Nishiyama, T. Inoue and T. Irifune, *Inorg. Chem.*, 2013, **52**, 1604–1609.
13 Y. Sakai, *et al.*, *J. Am. Chem. Soc.*, 2017, **139**, 4574–4581.
14 G. Shimura, Y. Shirako, K. Niwa and M. Hasegawa, *J. Solid State Chem.*, 2016, **242**, 55–62.
15 A. Deschanvres, B. Raveau and F. Tollemer, *Bull. Soc. Chim. Fr.*, 1967, 4077–4078.
16 A. A. Belik, Y. Matsushita and D. D. Khalyavin, *Angew. Chem., Int. Ed.*, 2017, **56**, 10423–10427.
17 I. Yamada, *Sci. Technol. Adv. Mater.*, 2017, **18**, 541–548.
18 G. Shimura, K. Niwa, Y. Shirako and M. Hasegawa, *Eur. J. Inorg. Chem.*, 2017, 835–839.
19 K. Leinenweber and J. Parise, *J. Solid State Chem.*, 1995, **114**, 277–281.
20 N. Yao, A. Navrotsky and K. Leinenweber, *J. Solid State Chem.*, 1996, **123**, 73–82.
21 A. Aimi, D. Mori, K. Hiraki, T. Takahashi, Y. J. Shan, Y. Shirako, J. S. Zhou and Y. Inaguma, *Chem. Mater.*, 2014, **26**, 2601–2608.
22 E. Solana-Madruga, A. M. Arevalo-Lopez, A. J. Dos Santos-Garcia, E. Urones-Garrote, D. Avila-Brande, R. Saez-Puche and J. P. Attfield, *Angew. Chem., Int. Ed.*, 2016, **55**, 9340–9344.
23 L. Zhang, Y. Matsushita, K. Yamaura and A. A. Belik, *Inorg. Chem.*, 2017, **56**, 5210–5218.
24 G. M. McNally, A. M. Arévalo-López, P. Kearins, F. Orlandi, P. Manuel and J. P. Attfield, *Chem. Mater.*, 2017, **29**, 8870–8874.
25 A. A. Belik, Y. Matsushita, M. Tanaka and E. Takayama-Muromachi, *Chem. Mater.*, 2012, **24**, 2197–2203.
26 A. A. Belik and W. Yi, *J. Phys.: Condens. Matter*, 2014, **26**, 163201.
27 (*a*) W. M. Reiff, K. Leinenweber and J. Parise, *Mater. Res. Soc. Symp. Proc.*, 1997, **453**, 387–392; (*b*) H. Li, S. Liu, L. Chen, C. Li and Z. Wang, *Physica E*, 2015, **69**, 133–137.
28 J. Ruiz-Fuertes, T. Bernert, D. Zimmer, N. Schrodt, M. Koch-Muller, B. Winkler, L. Bayarjargal, C. Popescu, S. MacLeod and K. Glazyrin, *Phys. Rev. B*, 2017, **96**, 094101.
29 G. Y. Gou, N. Charles, J. Shi and J. M. Rondinelli, *Inorg. Chem.*, 2017, **56**, 11854–11861.
30 L. Zhang, Y. Matsushita, K. Yamaura and A. A. Belik, unpublished results.
31 Y. S. Glazkova, N. Terada, Y. Matsushita, Y. Katsuya, M. Tanaka, A. V. Sobolev, I. A. Presniakov and A. A. Belik, *Inorg. Chem.*, 2015, **54**, 9081–9091.
32 A. A. Belik, Y. S. Glazkova, Y. Katsuya, M. Tanaka, A. V. Sobolev and I. A. Presniakov, *J. Phys. Chem. C*, 2016, **120**, 8278–8288.
33 Y. Akizuki, I. Yamada, K. Fujita, K. Taga, T. Kawakami, M. Mizumaki and K. Tanaka, *Angew. Chem., Int. Ed.*, 2015, **54**, 10870–10874.
34 R. D. Shannon, *Acta Crystallogr., Sect. A: Cryst. Phys., Diffr., Theor. Gen. Crystallogr.*, 1976, **32**, 751–767.
35 J. Sanchez-Benitez, J. A. Alonso, M. J. Martinez-Lope, A. de Andres and M. T. Fernandez-Diaz, *Inorg. Chem.*, 2010, **49**, 5679–5685.
36 M. Sato and Y. Hama, *J. Mater. Chem.*, 1993, **3**, 233–236.
37 J. Li, M. A. Subramanian, H. D. Rosenfeld, C. Y. Jones, B. H. Toby and A. W. Sleight, *Chem. Mater.*, 2004, **16**, 5223–5225.
38 I. Yamada, M. Murakami, N. Hayashi and S. Mori, *Inorg. Chem.*, 2016, **55**, 1715–1719.
39 D. Waroquiers, X. Gonze, G.-M. Rignanese, C. Welker-Nieuwoudt, F. Rosowski, M. Göbel, S. Schenk, P. Degelmann, R. André, R. Glaum and G. Hautier, *Chem. Mater.*, 2017, **29**, 8346–8360.
40 M. A. Subramanian, D. Li, N. Duan, B. A. Reisner and A. W. Sleight, *J. Solid State Chem.*, 2000, **151**, 323–325.
41 S.-H. Byeon, M. W. Lufaso, J. B. Parise, P. M. Woodward and T. Hansen, *Chem. Mater.*, 2003, **15**, 3798–3804.
42 T. Saito, R. Yamada, C. Ritter, M. S. Senn, J. P. Attfield and Y. Shimakawa, *Inorg. Chem.*, 2014, **53**, 1578–1584.
43 H. Okamoto, M. Karppinen, H. Yamauchi and H. Fjellvag, *Solid State Sci.*, 2009, **11**, 1211–1215.
44 S. V. Streltsov and D. I. Khomskii, *Phys. Rev. B: Condens. Matter Mater. Phys.*, 2014, **89**, 201115.
45 A. Prodi, A. Daoud-Aladine, F. Gozzo, B. Schmitt, O. Lebedev, G. van Tendeloo, E. Gilioli, F. Bolzoni, H. Aruga-Katori, H. Takagi, M. Marezio and A. Gauzzi, *Phys. Rev. B: Condens. Matter Mater. Phys.*, 2014, **90**, 180101.
46 A. A. Belik, Y. Matsushita, Y. Kumagai, Y. Katsuya, M. Tanaka, S. Yu. Stefanovich, B. I. Lazoryak, F. Oba and K. Yamaura, *Inorg. Chem.*, 2017, **56**, 12272–12281.
47 S. G. Ebbinghaus, *Prog. Solid State Chem.*, 2007, **35**, 421–431.
48 S. V. Ovsyannikov, A. M. Abakumov, A. A. Tsirlin, W. Schnelle, R. Egoavil, J. Verbeeck, G. Van Tendeloo, K. V. Glazyrin, M. Hanfland and L. Dubrovinsky, *Angew. Chem., Int. Ed.*, 2013, **52**, 1494–1498.
49 M. A. Subramanian, *J. Solid State Chem.*, 1994, **111**, 134–140.
50 Y. Shimoda, Y. Doi, M. Wakeshima and Y. Hinatsu, *J. Solid State Chem.*, 2010, **183**, 1962–1969.
51 Z. Y. Li, *et al.*, *J. Am. Chem. Soc.*, 2018, DOI: 10.1021/jacs.7b11219.